https://doi.org/10.1016/j.ijheatmasstransfer.2016.04.001

This is the Pre-Published Version.

Title: A new analytical solution for horizontal geothermal heat exchangers with vertical spiral coils

Authors: Deqi Wang[a], Lin Lu[a,*] and Ping Cui[b,c]

[a] Renewable Energy Research Group, The Hong Kong Polytechnic University, Hong Kong, China

[b] Key Laboratory of Renewable Energy Utilization Technologies in Buildings, Ministry of Education, Jinan, China

[c] School of Thermal Energy Engineering, Shandong Jianzhu University, Jinan, China

*Corresponding author

Tel.: +852-3400 3596; Fax: +852-2765 7198.

E-mail address: vivien.lu@polyu.edu.hk.

Keywords: Ground-coupled heat pump, Spiral heat exchanger, Heat transfer, Analytical solution

© 2016. This manuscript version is made available under the CC-BY-NC-ND 4.0 license https://creativecommons.org/licenses/by-nc-nd/4.0/

Abstract

Horizontal geothermal heat exchangers (HGHEs) with vertical spiral coils have been increasingly used in ground source heat pump (GSHP) systems. Research studies have been conducted using field tests and simulations trying to reveal the heat transfer mechanism of HGHEs with vertical spiral coils and to provide a good heat transfer performance. However, there is no analytical solution has been established for HGHEs with vertical spiral coils. Of particular interest is the temperature variation at the soil surface. The study presented in this paper proposes the development of a mathematical vertical ring-coil model used to describe the heat transfer process of HGHEs with vertical spiral coils. In this new model, the spiral heat exchanger is simplified as a series of ring coils that inject/extract heat in/from a semi-infinite medium. A single ring model in an infinite medium is first introduced. Using images and superposition, a multiple ring-coils analytical solution is then given. The significant influence on the heat transfer performance of HGHEs temperature variation of the ground surface is then considered. A periodically changed boundary condition is being taken into consideration in the modeling process. The validity of the model was examined by a field test and a 3-D simulation model. The analytical solutions may provide a desirable and better tool for the simulation/design HGHEs with vertical spiral coils.

1 Introduction

Currently the ground-coupled heat pump (GCHP) system is widely used in commercial or residential buildings for cooling, heating and hot water application. Compared with the air source systems, the GCHP has advantages as regards electricity consumption, maintenance cost and environmental protection [1]. A GCHP system typically includes a geothermal heat exchanger (GHEs) system, a heat pump unit and a heat distribution terminal system. GHE is the key connecting device between the heat pump unit and ground sources and as such is regarded as the most important component of a GCHP system in both the design or construction stages. In general, the typical geothermal heat exchangers could be divided into two groups: the vertical ground heat exchangers (VGHEs) and the horizontal ground heat exchangers (HGHEs) [2]. VGHEs are usually used in urban area, but its high installation cost makes this types of heat exchangers hardly be widely used on the market. HGHEs, with the advantage of low installation cost, provide an alternative GHE solution in suburbs with sufficient land area such as golf courses, farms and rural cottages. The HGHE system is usually buried in a shallow trench with a configuration of single/multiple linear pipe or spiral-types pipes as shown in Figure 1.

Figure 1 Schematics of different geothermal heat exchangers

To improve GCHP reliability and optimize their operation, much research has been conducted to investigate the GHE heat transfer process and many advanced analytical models have been developed for VGHEs, in addition to both experimental and numerical studies [3-5]. Of particular note is the pile geothermal heat exchanger [6, 7]. However, few studies based on HGHEs have been reported and of these most were focused on experiment analysis or numerical simulation. Demir et al. [8] established a 2-D numerical model to estimate the temperature response of straight linear HGHEs. A heat flux boundary condition was applied on the ground surface to simulate the influence of temperature change [8]. A simplified 3-D numerical model was developed by Congedo et al. with the aim of investiaging the heat transfer efficiency of HGHEs, using different configurations. It was found that the vertical spiral HGHEs enabled a stronger heat transfer performance than that of the the linear and slinky HGHEs [9]. This finding was further confirmed by field tests [10]. The first HGHE analytical model was developed by Ingersoll and Plass in 1948 [11]. In this model, the straight linear HGHE was regarded as an infinite line heat source injecting/extracting heat into/from an infinite medium. Ground surface temperature fluctuation was neglected in the modeling process. Mei et al. [12] then, proposed a modified infinite line model in a semi-infinite medium. This model was still only used for straight linear HGHEs and likewise neglected the surface temperature variation [12]. A ring source model is possibly the latest development. The slinky-loops was separated into a series of separated ring coils [13], and shows a good daily performance [14]. However, as with the semi-infinite model, this ring source model also assumed the ground surface temperature boundary to be constant temperature boundary.

According to previous studies, no reliable analytical model, to describe the heat transfer behavior of HGHEs with vertical spiral coils, is available. Compared with straight linear and slinky-loop HGHEs, HGHEs with vertical spiral pipes have a short application history. However, due to the higher heat transfer efficiency and less land area requirements, the vertical spiral heat exchanger have been attracting a recent increased interest [9]. But due to the complex configuration of the vertical spiral pipes, the previous analytical models of HGHE failed to describe its heat transfer process. Hence, a need for a new analytical model has been recognized for the design/simulation of vertical spiral HGHEs. Additionally, it is well noted that the temperature of the soil surrounding the HGHEs is sensitively affected by the temperature of the ground surface, and also has the ability to quickly retrieve its original temperature once cooling or heating operations have ceased [15]. Thus, it is important to take the temperature fluctuations of the ground surface into consideration during the heat transfer modeling process [16]. Accordingly, the boundary solution for vertical spiral HGHEs should be also derived.

Therefore, the aim of the study presented in this paper is to provide a methodology to enable a theoretical analysis of the heat transfer process of vertical spiral HGHEs. To achieve this, a vertical ring-coil model has been developed based on Green's function theory. In this new model, the spiral heat exchanger is simplified to form a series of ring coils that inject/extract heat in/from a semi-infinite medium. A single ring model in an infinite medium is first introduced. Based on the method of images and superposition, the multiple ring-coils analytical solution is then, given. As the temperature variation of the ground surface has a significant influence on the heat transfer performance of HGHEs, a sinusoidal temperature boundary condition is taken into consideration in the modeling process. To validate this new model, the on-site experiment and the proposed analytical model are compared. In addition, a numerical simulation model, based on the finite element method, has also been used to verify the long-term operation of the model. Two validation processes were conducted and a good agreement was shown. Finally, the temperature responses of different surface conditions were calculated by means of a valid analytical model and further discussed.

2 Ring-coil heat source solution

Taking the geometrical features of vertical spiral HGHEs and the impact of surface temperature into account, a new model, i.e. the vertical ring coils source model, is established. The vertical spiral HGHE was represented by a series of separated rings with a radius $\boldsymbol{r_0}$ and pitch $\boldsymbol{b}$ being coincident with the y-axis. In line with the assumptions in previous analytical models of geothermal heat exchangers [13, 17], the ground is assumed to be a homogeneous medium with thermal properties remaining constant in the face of temperature change. The initial temperature of the ground soil is assumed to be uniform and constant. Based on the transient heat conduction equation and with the given assumptions and initial conditions, this heat conduction problem can be expressed as follows:

$$
\begin{aligned}
&\frac{\partial^2\theta}{\partial x^2}+\frac{\partial^2\theta}{\partial y^2}+\frac{\partial^2\theta}{\partial z^2}+\frac{1}{k}g\left(x,y,z,t\right)=\frac{1}{\alpha}\frac{\partial\theta}{\partial t}, && \text{in} \quad -\infty<x<+\infty,\ -\infty<y<+\infty,\\
& && \qquad 0\le z<+\infty,\ t>0\\
&\theta=A\cdot\sin(\omega t+\varepsilon), && \text{at} \quad z=0,\ t>0\\
&\theta=0, && \text{for} \quad t=0,\ \text{in the region}
\end{aligned}
\tag{1}
$$

According to Green's function theory [18], the temperature response can be obtained by dividing the equation into energy generation, $\theta_g(x,y,z,t)$ and the boundary , $\theta_{b,c}(x,y,z,t)$, as shown in Eq.(2).

$$\theta(x,y,z,t)=\theta_g(x,y,z,t)+\theta_{b,c}(x,y,z,t)$$
$$\theta_g(x,y,z,t)=\int_{\tau=0}^{t}\int_R \frac{\alpha}{k}G\left(x,y,z,t\middle|x',y',z',\tau\right)g\left(x',y',z',\tau\right)dv'd\tau \qquad (2)$$
$$\theta_{b,c}(x,y,z,t)=-\alpha\int_{\tau=0}^{t}\sum_{j=1}^{s}\int_{S_j} f_j\left(\mathbf{r}_j^{'},\tau\right)\frac{\partial G}{\partial n_j^{'}}\Big|_{r'=r_j^{'}}ds_j^{'}d\tau$$

Before developing the ring-coil model, a simple model, i.e. the single ring-coil heat source model with zero surface temperature, is first introduced as the basic function of the horizontal ring-coil model.

2.1 Single ring-coil heat source in a semi-infinite medium

The temperature response at points (*x*, *y*, *z*) for an impulse heat source located at (*x'*, *y'*, *z'*) in an infinite solid with zero initial temperature at an initial time of τ can be expressed as:

$$\theta_p\left(x,y,z,t\right)=\frac{1}{8\left[\pi\alpha\left(t-\tau\right)\right]^{3/2}}\exp\left[-\frac{\left(x-x'\right)^2+\left(y-y'\right)^2+\left(z-z'\right)^2}{4\alpha\left(t-\tau\right)}\right] \qquad (3)$$

Thus, the temperature increase due to a single ring source can be obtained by integrating the point source along a ring circle:

$$\theta_{rsi,c}\left(x,y,z,t\right)=\int_{\tau=0}^{t}\int_l \frac{\alpha}{k}G_{in}\left(x,y,z,t\middle|x',y',z',\tau\right)g\left(x',y',z',\tau\right)ds'd\tau$$
$$G_{in}\left(x,y,z,t\middle|x',y',z',\tau\right)=\frac{1}{8\left[\pi\alpha\left(t-\tau\right)\right]^{3/2}}\exp\left[-\frac{\left(x-x'\right)^2+\left(y-y'\right)^2+\left(z-z'\right)^2}{4\alpha\left(t-\tau\right)}\right]$$

(4)

Assuming the ring source releases heat with a strength of $q_r r_0$ with a center point (0, 0, v_c) and a radius of r_0 on the surface of $y=0$, as shown in Figure 2, the temperature at points (*x*, *y*, *z*) at time *t* can be expressed as:

$$\theta_{rsi,c}\left(x,y,z,t\right)=q_r\frac{\alpha}{k}\int_0^t\int_0^{2\pi}\frac{r_0}{8\left[\pi\alpha\left(t-\tau\right)\right]^{3/2}} \times\exp\left[-\frac{\left(x-r_0\sin\sigma\right)^2+y^2+\left(z-r_0\cos\sigma-v_c\right)^2}{4\alpha\left(t-\tau\right)}\right]d\sigma d\tau = \frac{q_r r_0}{4\pi k}\int_0^{2\pi}\frac{1}{r_*}ercf\left(\frac{r_*}{\sqrt{4\alpha t}}\right)d\sigma \quad (5)$$

where $ercf(u)=2/\pi\int_u^{\infty}\exp(-\beta^2)\,d\beta$ is the error function and r_* is the distance between the observation point and heat source, which can be written as $r_*=\sqrt{\left(x-r_0\sin\sigma\right)^2+y^2+\left(z-r_0\cos\sigma-v_c\right)^2}$.

Figure 2 Schematic representation of signal ring-coil in an infinite medium

The image method is applied to find the single ring source in a semi-infinite medium. As shown in Figure 3, a virtual ring source with the same geometry is applied symmetrically over the boundary surface. The heat discharging rate of the virtual ring source is considered to be the opposite of the original one.

Figure 3 Schematic representation of signal ring-coil in a semi-infinite medium

By applying this virtual ring source, the temperature at the ground surface is always maintained as zero. Therefore, the temperature rise of the single ring source in a semi-infinite medium can be obtained directly by superposing the solution of a virtual ring source into Eq. (5). The temperature at points (*x*, *y*, *z*) at time *t* can then be expressed as:

$$\theta_{rss,c}\left(x,y,z,t\right)=\int_{\tau=0}^{t}\int_l\frac{\alpha}{k}G_{sin}\left(x,y,z,t\middle|x',y',z',\tau\right)g\left(x',y',z',\tau\right)ds'd\tau \quad (6)$$

$$G_{sin}\left(x,y,z,t\middle|x',y',z',\tau\right)=\frac{1}{8\left[\pi\alpha\left(t-\tau\right)\right]^{3/2}}\exp\left[-\frac{\left(x-x'\right)^2+\left(y-y'\right)^2}{4\alpha\left(t-\tau\right)}\right]\times\left\{\exp\left[-\frac{\left(z-z'\right)^2}{4\alpha\left(t-\tau\right)}\right]-\exp\left[-\frac{\left(z+z'\right)^2}{4\alpha\left(t-\tau\right)}\right]\right\} \quad (7)$$

By using the error function to simplify these equations, the temprature can then, be written as:

$$\begin{cases}\theta_{rs,c}\left(x,y,z,t\right)=\dfrac{q_r r_0}{4k\pi}\displaystyle\int_0^{2\pi}\frac{1}{r_+}erfc(\frac{r_+}{\sqrt{4\alpha t}})-\frac{1}{r_-}erfc(\frac{r_-}{\sqrt{4\alpha t}})\,d\sigma \\ r_+=\sqrt{\left(x-r_0\sin\sigma\right)^2+y^2+\left(z-r_0\cos\sigma-v_c\right)^2} \\ r_-=\sqrt{\left(x-r_0\sin\sigma\right)^2+y^2+\left(z+r_0\cos\sigma+v_c\right)^2}\end{cases} \quad (8)$$

By introducing the following dimensionless variables: $Fo=\alpha t/r_0^2$, $\Theta=k\theta r_0/q$, $V=v_c/r_0$, $X=x/r_0$, $Y=y/r_0$, $Y'=y_0/r_0$, $Z=z/r_0$, the dimensionless temperature can be rewritten as a function of the following:

$$\begin{cases}\Theta_{rs,c}=\dfrac{1}{4\pi}\displaystyle\int_0^{2\pi}\frac{1}{R_+}erfc(\frac{R_+}{\sqrt{4Fo}})-\frac{1}{R_-}erfc(\frac{R_-}{\sqrt{4Fo}})\,d\sigma \\ R_+=\sqrt{\left(X-\sin\sigma\right)^2+Y^2+\left(Z-\cos\sigma-V\right)^2} \\ R_-=\sqrt{\left(X-\sin\sigma\right)^2+Y^2+\left(Z+\cos\sigma+V\right)^2}\end{cases} \quad (9)$$

Figure 4 Dimensionless temperature response with different ***Fo***

2.2 Multiple ring-coils source model

The superposition method is used to obtain the analytical solution of the multiple ring-coil source model. In the multiple ring-coil model, the vertical spiral HGHEs are assumed to be a series of ring-coil sources buried in a semi-infinite medium. The distance between two neighboring ring coils are assumed to be the same with the spiral pitch of the spiral heat exchanger. The number of ring-coils (N) is equal to the ratio of the trench length to the spiral pitch of the spiral heat exchanger.

Figure 5 Schematic representation of horizontal ring-coil source model

The multiple ring-coils source model with a zero surface temperature solution can be regarded as the superposition of a single sing-coil source model with finite times:

$$\begin{aligned}\theta_{mrs,c}\left(x,y,z,t\right)=q_r\frac{\alpha}{k}\sum_{n=0}^{N-1}\int_0^t\int_0^{2\pi}&\frac{r_0}{8\left[\pi\alpha\left(t-\tau\right)\right]^{3/2}}\\ &\times\exp\left[-\frac{\left(x-r_0\sin\sigma\right)^2+(y-nb)^2+\left(z-r_0\cos\sigma-v_c\right)^2}{4\alpha\left(t-\tau\right)}\right]d\sigma d\tau\end{aligned} \tag{10}$$

$$\begin{cases}\theta_{mrs,c}\left(x,y,z,t\right)=\dfrac{q_r r_0}{4k\pi}\displaystyle\sum_{n=0}^{N-1}\int_0^{2\pi}\frac{1}{r_{n+}}erfc\left(\frac{r_{n+}}{\sqrt{4\alpha t}}\right)-\frac{1}{r_{n-}}erfc\left(\frac{r_{n-}}{\sqrt{4\alpha t}}\right)\,d\sigma\\ r_+=\sqrt{\left(x-r_0\sin\sigma\right)^2+\left(y-nb\right)^2+\left(z-r_0\cos\sigma-v_c\right)^2}\\ r_-=\sqrt{\left(x-r_0\sin\sigma\right)^2+\left(y-nb\right)^2+\left(z+r_0\cos\sigma+v_c\right)^2}\end{cases} \tag{11}$$

Define $B=b/r_0$, then Eq. (11) can be rewritten as follow:

$$\begin{cases}\Theta_{mr,c}=\dfrac{1}{4\pi}\displaystyle\sum_{n=0}^{N-1}\int_0^{2\pi}\frac{1}{R_+}erfc\left(\frac{R_{n+}}{\sqrt{4Fo}}\right)-\frac{1}{R_-}erfc\left(\frac{R_{n-}}{\sqrt{4Fo}}\right)\,d\sigma\\ R_{n+}=\sqrt{\left(X-\sin\sigma\right)^2+\left(Y-nB\right)^2+\left(Z-\cos\sigma-V\right)^2}\\ R_{n-}=\sqrt{\left(X-\sin\sigma\right)^2+\left(Y-nB\right)^2+\left(Z+\cos\sigma+V\right)^2}\end{cases} \tag{12}$$

2.3 Solution of surface boundary

It is well known that the temperature of the ground surface changes periodically during the whole year and that this temperature change has a great impact on the operation of the horizontal heat exchangers [19]. Therefore, it is essential to take the boundary influence into consideration when estimating the heat transfer performance. Based on Green's function theory, the solution of the surface boundary can be obtained from the derivative of the Eq. (7):

$$\frac{\partial G_{sin}}{\partial z'}\bigg|_{z'=0} = \frac{z}{8(\pi)^{3/2}\left[\alpha(t-\tau)\right]^{5/2}}\exp\left[-\frac{(x-x')^2+(y-y')^2+z^2}{4\alpha(t-\tau)}\right] \tag{13}$$

The temperature solution of the boundary condition will then, be obtained after computing the integral of the ground surface:

$$\begin{aligned}\theta_{b,c}(x,y,z,t) &= -\alpha\int_{\tau=0}^{t}\sum_{j=1}^{s}\int_{S_j} f_j\left(\mathbf{r}_j',\tau\right)\frac{\partial G}{\partial n_j'}\bigg|_{r'=r_j'} ds_j' d\tau \\ &= \alpha\int_{\tau=0}^{t}\int_{-\infty}^{\infty}\int_{-\infty}^{\infty} f(\tau)\frac{z}{8(\pi)^{3/2}\left[\alpha(t-\tau)\right]^{5/2}}\exp\left[-\frac{z^2+(y-y')^2+(x-x')^2}{4\alpha(t-\tau)}\right]dy'dx'd\tau \\ &= \alpha\int_{\tau=0}^{t} f(\tau)\frac{z}{2\sqrt{\pi}\left[\alpha(t-\tau)\right]^{3/2}}\exp\left[\frac{-z^2}{4\alpha(t-\tau)}\right]d\tau\end{aligned} \tag{14}$$

Assuming the surface temperature conforms to the rule of sine function, $f(\tau) = A\cdot\sin(\omega t+\varepsilon)$, this boundary solution can be solved by Laplace method [20]:

$$\theta_{b,c}(z,t) = A\cdot\exp(-z\sqrt{\frac{\omega}{2\alpha}})\cdot\sin(\omega t+\varepsilon - z\sqrt{\frac{\omega}{2\alpha}}) + \frac{2\alpha A}{\pi}\int_0^\infty \frac{\omega\cos(\varepsilon)-\alpha\mu^2\sin(\varepsilon)}{\omega^2+\alpha^2\mu^4}\exp(-\alpha\mu^2 t)\sin(\mu z)\mu d\mu \tag{15}$$

The boundary solution independents with *x* and *y*, related to only the depth of the observation point. The second term in Eq.(15) caused by the uniform initial temperature and dies away as time increases, leaving the steady fluctuation of period $2\pi/\omega$.

3 Numerical and experimental validation

Both numerical and experimental methods were used to validate the new horizontal ring-coil model. The experimental method is reliable but hard to monitor the temperature response of every point in the heat transfer medium. Besides, collecting long-term operation data always takes several years. Thus, to save the time cost, a numerical model is established by finite element method.

3.1 On-site experiment

The test rig was established based on a solar-hybrid GCHP system on the campus of Shandong Jianzhu University, China in 2012. The system mainly consists of a water-refrigerant heat pump unit, GHEs, solar collectors of 12 m^2, a thermal storage tank with 800 liters and a data collection system. There are two typical GHE systems, i.e. vertical GHEs with 12 boreholes and a vertical spiral HGHE. For the spiral heat exchanger, the dimensions of the spiral radius and the spiral pitch are the same as 0.4m. The horizontal heat exchanger is buried in a 12m-long trench with the depth of 2.0m. The buried tubes are high-density polyethylene pipe with outer diameter of 32mm. The experiment was carried out on 8th Jun 2015.

The performance of the spiral HGHEs was monitored by a data collection system. As shown in Figure 6, three temperature sensors (Pt100) were installed at the pipes wall to measure the temperatures at the inlet, the middle point and the outlet of the heat exchanger. Additionally, in the ground soil, a temperature sensor was installed 1m below the ground surface at the central of the trench. All the Pt100 sensors have an accuracy of ±0.1℃. The water flow rate was measured by a flow meter, whose flow range is within 0.2-2 m^3/h, and the flow meter has been calibrated by the manufacturer to ±0.5% of full scale.

Figure 6 Schematic representation of the experiment (a) and a photo of the on-site spiral heat exchanger (b).

3.2 3-D simulation model

As the numerical model is hardly to fully model the transient heat transfer process of the HGHEs, simplifying assumptions are necessary before establishing the numerical model. Similar to the simplification in the analytical model, the ground is regarded as a homogeneous medium, and its thermal properties are independent of temperature. Table 1 shows the main parameters used in the simulation model. Additionally, for numerical simulation, a large finite domain was established to represent the semi-infinite ground. The dimensions of this finite domain should be sufficient to ensure that the heat exchanger has no thermal influence on the domain boundary within the concerned time.

Table 1 Physical properties used in the numerical model for model validation

As shown in Figure 7 (a), the calculation domain for this simulation was regarded as a parallelepiped of 32m (length) × 15m (width) × 9m (depth). The spiral heat exchanger simulated here is a circular pipe with 25.3-m-long. The spiral radius and pitch of this spiral heat exchanger are assumed to be 0.4m. The central axis of this heat exchanger is buried at 1.0 m under the ground surface. In order to validate the boundary solution, the temperature of the ground surface is expressed as a sinusoidal function:

$$\theta_b = 15 \cdot \sin(\frac{2\pi}{365 \times 24 \times 3600} t + 0.47\pi) \qquad (16)$$

Except for the boundary of ground surface, all the other boundary conditions are thermally insulated. The heat transfer process between circulating water and the sourrounding soil is simplified as a heat conduction process with a line source discharging heat along the spiral heat exchanger.

Figure 7 Schematic representation of the simulation (a) and magnification of the mesh adjacent to the heat exchanger (b).

This heat transfer problem is solved with the commercial code, ANSYS CFX, and ICEM is used to generate the 3D mesh. The dense mesh is applied near the heat exchange wall and relatively loose mesh is used to the ground domain. 16,685,436 tetrahedral meshes are created in this simulation model.

4 Comparisons and discussion

4.1 Comparisons of the new ring-coils source model and on-site experiment

The tested heat transfer rates of the horizontal ring-coils heat exchanger are given in Figure 8. As shown in this figure, the heat injection curve dropped to zero several times during the operation time. The first two times were caused by the manual intervention and the others were controlled by the system which should be the consequence of cooling demand decreasing. However, it should point out that the injection rate, calculated by the water flux and the temperature difference between inlet and outlet of the heat exchanger, cannot accurately represent the real heat transfer process. For example, when the circulation pump was shut down, the water flux became zero, so the measured injection rate became zero. But, in the realty, the high heat capacity of water makes the heat exchanger continuously release heat into the ground after the circulation pump shutdown until the temperature of water was the same as the one of surrounding ground. The measured heat injection rate fluctuated greatly with the operation time, which requires a great deal of discrete points to fully simulate it. Thus, to save the calculation time, a series of average heat pulses by taking an average in every ten minutes, was applied in the predicted calculation.

Figure 8 Illustration of the heat injection rate during the cooling operation

Figure 9 illustrates the comparisons between the predicted and measured pipe wall temperatures at the middle monitoring point. It can be seen from this figure, besides a large relative error at the beginning, the general variation trends of the experimental and analytical models agree well during the operating time. The relative error is defined in Eq.17 to better analyze the difference between these two methods.

$$\text{Relative error} = \frac{\text{Analytical value - Experimental value}}{\text{Experimental value - Initial value}} \tag{17}$$

Figure 9 Soil temperature determined by experiment test and analytical calculation

It can be seen that, from Figure 9, the maximum relative error is less than 25% after the initiative period, which may be acceptable for the practicable engineering. The temperature rise calculated from these two methods shows a small difference at the beginning of the test case, from 7:30 a.m. to 11:30 a.m. After that, an obvious difference occurs in the time period between 11:30 a.m. and 13:30 p.m. The analytical results increase continuously while the measured temperature decreases slightly during this operation time. Generally, under a uniform thermal excitation of the heat souse, the temperature should keep growing until the heat transfer process becomes stable. The heat transfer process usually takes a long-time to approach the stable stage, so, obviously, the temperature of the pipe wall should increase during this short operation time, as presented by analytical results. According to the meteorological records, there was a shower rain in the night before the field test. Thus, a possible interpretation for the experimental results is that a part of heat energy was taken away by the rainwater infiltration. The temperature rise may be prevented by the rainwater infiltration. Additionally, compared with the measured data, the analytical value of the temperature rise on the pipe wall fluctuated more sharply when the heat injection rate was unstable.

This can be observed between 18:30 p.m. to 21:30 p.m. This is due to the assumption of the line source in the center of the heat exchanger pipe, which neglects the physical size and specific heat of the circulating water.

4.2 Comparisons of the new analytical model and the proposed numerical model

In order to determine the long-term performance of this new ring-coils model, a comparison is conducted between the numerical model and the vertical ring-coils source model. Taking an example of N=8 and maintaining the ground surface temperature as zero, the pipe wall temperatures located at the middle of vertical spiral HGHEs are illustrated in Figure 10. These representative temperature rise obtained from the numerical and analytical methods. It can be seen that the analytical results (A-N8) match perfectly with the numerical results (N-N8). After a rapid growth, the temperature begins to stabilize. Obviously, compared with the shorter horizontal heat exchanger (A-N1), the longer one (A-N32) takes less time to reach the steady-stage. But, in this case, when the number of ring-coils is larger than 40, the influence of the pipe length becomes insignificant.

Figure 10 Variations of dimensionless temperature responses calculated by analytical and numerical methods with ***Fo*** with different numbers of coils

For the horizontal heat exchanger with N=8, the temperature response on the pipe wall alone the axis direction with different instants are calculated and plotted in Figure 11. As shown in this figure, for the case of Fo=1, the analytical and the numerical results agree well with each other. Eight peak values are located at each ring coil. For a long-term operation, the temperature at the center of the spiral heat exchanger is remarkably higher than its top and bottom. Additionally, the structure simplification of the spiral heat exchanger becomes obvious when the Fourier number is large. The temperature rise calculated from the analytical model is lower than the simulation results at the top of the heat exchanger but higher at the bottom. Even though the analytical results show little difference with the numerical one in long-term operation, the relative error is quite small and the new analytical model is acceptable for engineering application.

Figure 11 Temperature profiles along the axial direction with different ***Fo*** (with x=0 and z=0.6 m).

The temperature rise under sinusoidal surface temperature (N-Sinusoidal BC) is also calculated and plotted in Figure 12. Compared with the results from zero surface temperature, the temperature response is greatly changed by the sinusoidal surface temperature. The temperature becomes steady after a few days for the case of zero surface temperature, but the pipe temperature fluctuates significantly for the sinusoidal case. Under the sinusoidal surface temperature condition, the analytical solution is matched well with the numerical one, which means that the boundary solution is reliable.

Figure 12 Temperature response calculated by analytical and numerical method with sinusoidal surface temperature (with x=0, y=1.2 and z=0.6m).

4.3 Comparisons of the new analytical model with different boundary conditions

Taking a simple heat transfer design case into consideration, different boundary conditions, constant temperature and sinusoidal temperature are applied on the ground surface. It assumed that the heat pump operates at the cooling mode in the first three months, which means that the heat exchanger injects heat energy into the ground soil. The heat flow of the ring-coils source is assumed to be 50W per ring. Then, the system stops working in the next three months. After this recovery period, the heat exchanger extracts the heat from the ground to warm the indoor room. The heat extraction rate is considered as the same as the heat injection rate. After heating operation for three months, the system enters the next recovery period. According to the climatic data recorded in the year of 2014 by a meteorological station located at Jinan, China (latitude 36° 40′ north and longitude 117° 00′ east), a sinusoidal changed temperature was applied at the ground surface.

Figure 13 Annual climatic data, recorded by the climatic station, used as boundary conditions in the simulations

Figure 14 Illustration of the heat injection and extraction in one year

As shown in Figure 15, five points, at different depths below the ground surface, are selected to monitor the ground temperature variation during the heat injection/extraction of the spiral heat exchanger. These points are along the direction of the ground depth and the third point is located at the center of the fourth ring-coil.

Figure 15 Arrangement of monitoring points and the vertical heat exchanger.

Figure 16 shows the ground temperature profile under sinusoidal surface temperature but without heat source influence, which can be directly obtained by Eq. (15). Clearly, the ground temperature variation shows the feature of periodic changes, and the delayed effects can be easily observed with the depth increase. In addition, the point closer to the ground surface is more susceptible to the periodic temperature.

Figure 16 Soil temperature variation at different depths under sinusoidal surface temperature without heat source influence (with x=0m and y=1.2m).

By using the Eq. (10), the temperature rises with a constant surface temperature are calculated and plotted in Figure 17. As seen from this figure, in the heat injection stage, soil temperature increases rapidly from the initial temperature. Influenced by the boundary of constant temperature, the point near the ground surface easily becomes stable during the operation period. When the cooling operation ends, the ground temperature recovers gradually and the ground temperatures of all the points recover to the initial temperature at the end of the recovery stage. Then, in the following heating season and its recover period, because the heat transfer energy is same but in different directions, the trend of the temperature curve shows symmetrical distribution along *Y* axis with the value equal to the constant boundary temperature. It indicated that if the surface temperature unchanged during the operation, the heat pump, which not only provides cooling but also generates heating, can operate well in the whole year.

Figure 17 Soil temperature variation at different depths under constant surface temperature with heat injection/extraction (with x=0m and y=1.2m).

Figure 18 illustrates the temperature profile in different monitoring points by considering both the sinusoidal surface temperature and the season changed heat transfer condition. Obviously, the surface temperature greatly affects the temperature response of ground soil. Since the temperature of ground surface is much higher in the first three months, the ground temperature increases faster than those in Figure 17. Additionally, the temperature drops significantly in the heating operation season, and the temperature goes below zero in the medium-term in this season. The water cannot be used as circulating fluid in such medium-term season. The original heat transfer design is hardly to achieve under such local meteorological conditions, which means that the system may need more heat exchangers to meet the design requirement or the heating demand needs to be reduced to ensure system can operate normally.

Figure 18 Soil temperature variation at different depths under sinusoidal surface temperature with heat injection/extraction (with x=0m and y=1.2m).

Based on these calculation results, it can be seen that the surface temperature has a significant effect on the heat transfer performance of the horizontal heat exchangers and then influences the system efficiency of GCHP. The annual variation of the local ground surface temperature should be fully considered in designing the horizontal spiral heat exchangers.

5 Conclusions

Based on Green's function theory, a new analytical model, vertical ring-coil model, is established to better describe the heat transfer process of the horizontal geothermal heat exchangers with vertical spiral coils. In this new model, the ground was regarded as a semi-infinite medium and sinusoidal boundary condition was applied on the ground surface. A good agreement was shown in the comparisons between the results obtained from the on-site experiment and the proposed model, and the new analytical model was further validated by the numerical simulation. By using the new model, two different ground surface conditions (constant temperature and sinusoidal surface temperature) were calculated and compared. The results indicated that the surface temperature can directly influence the heat transfer performance of the horizontal heat exchangers, which should be fully considered in the system design. Because the proposed analytical model successfully takes the annual variation of surface temperature into consideration, the authors believe that this new model can provide a great aid to the engineers in designing and optimizing the size or arrangement of the horizontal geothermal heat exchangers with vertical spiral coils.

405 Nomenclature

Nomenclature			
x, y, z	cartesian coordinate (m)	Greek symbols	
X, Y, Z	dimensionless Cartesian coordinate	Θ	dimensionless excess temperature
v_c	buried depth of coils (m)	θ	excess temperature (℃)
b	coils pitch	σ	angle coordinate (rad)
r	radial coordinate (m)	τ	time (s)
r_0	coil radius (m)	ω	periodic coefficient
R	dimensionless radial coordinate	β, μ	Integral parameter
k	thermal conductivity (W m-1 K-1)	ε	initial phase angle (rad)
α	thermal diffusivity (m2 s-1)		
ρ	density (kg m-3)	Superscript	
c	specific heat (J kg-1 K-1)	$'$	integration parameter
q_r	heat extraction/injection per ring source	+	original heat source
t	time (s)	−	image heat source
A	temperature amplitude		
Fo	Fourier number		
N	numbers of ring-coils		

Acknowledgments

The work described in this paper is supported by a grant from Hong Kong Research Grant Council (RGC) Grand Research Funds B-Q31X, B-Q37H, Construction Industry Council through research grant of 5-ZJF2 and a grant from National Natural Science Foundation of China (Project No. 51208286).

Table

Table 1 Physical properties used in the numerical model for model validation

Parameters	Unit	Soil	Water
Density, ρ	Kg m^{-3}	3125	998
Heat capacity, *c*	J kg^{-1} K^{-1}	800	4182
Thermal conductivity, *k*	W m^{-1} K^{-1}	2.5	0.6069

Figures

Figure 1 Schematics of different geothermal heat exchangers

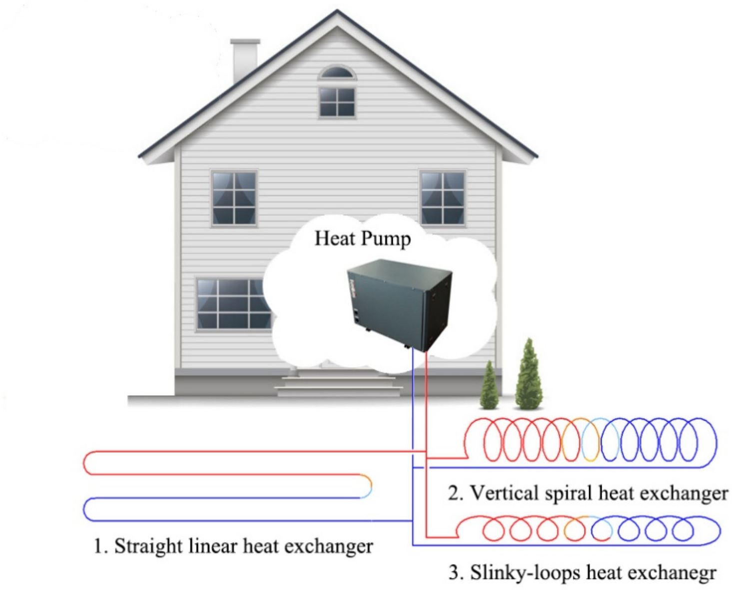

Figure 2 Schematic representation of signal ring-coil in an infinite medium

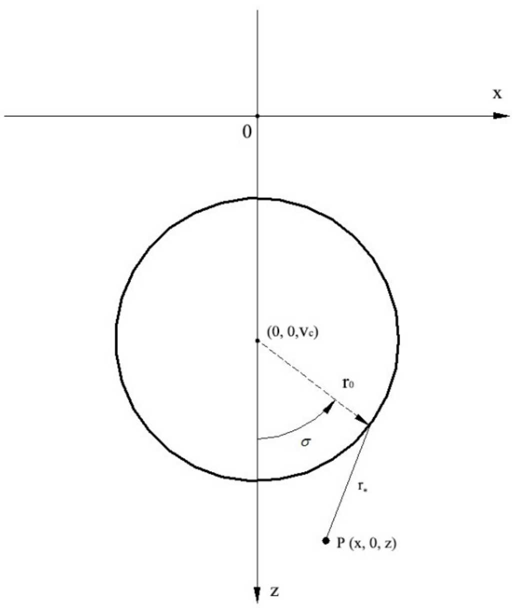

Figure 3 Schematic representation of signal ring-coil in a semi-infinite medium

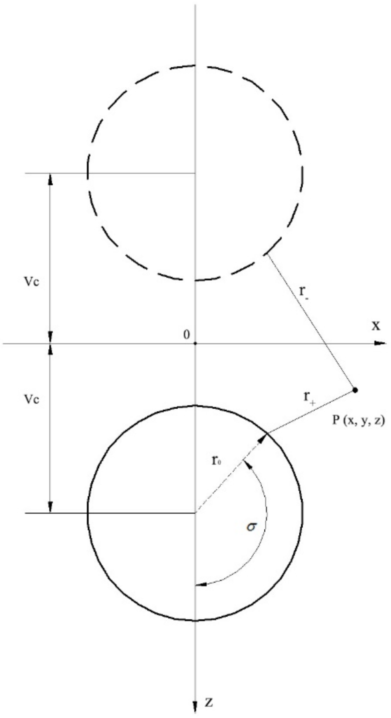

Figure 4 Dimensionless temperature response with different ***Fo***

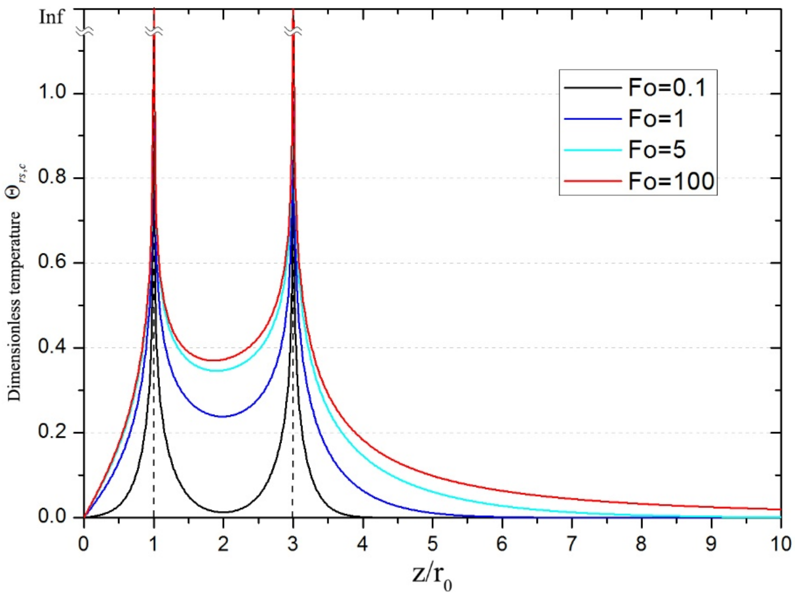

Figure 5 Schematic representation of horizontal ring-coil source model

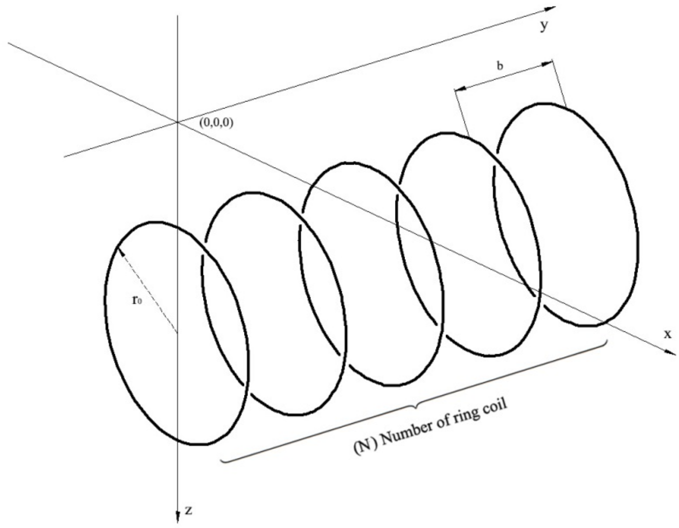

Figure 6 Schematic representation of the experiment (a) and a photo of the on-site spiral heat exchanger (b).

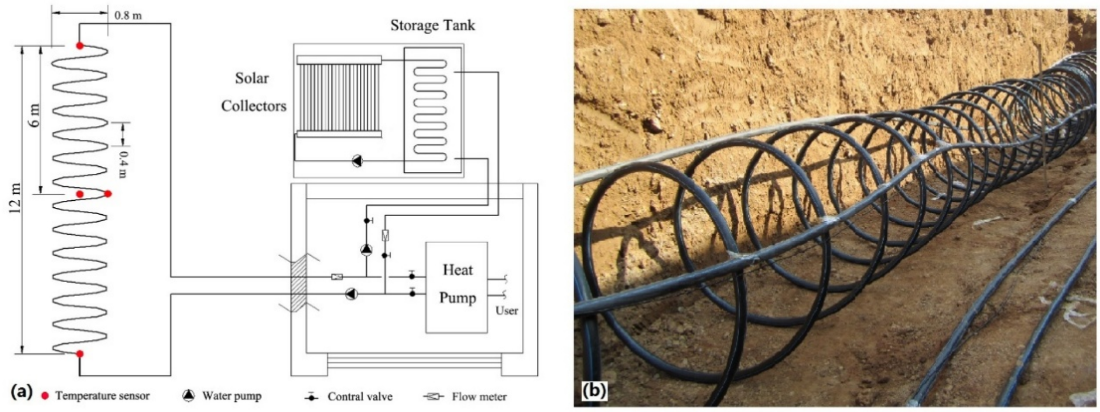

Figure 7 Schematic representation of the simulation (a) and magnification of the mesh adjacent to the heat exchanger (b).

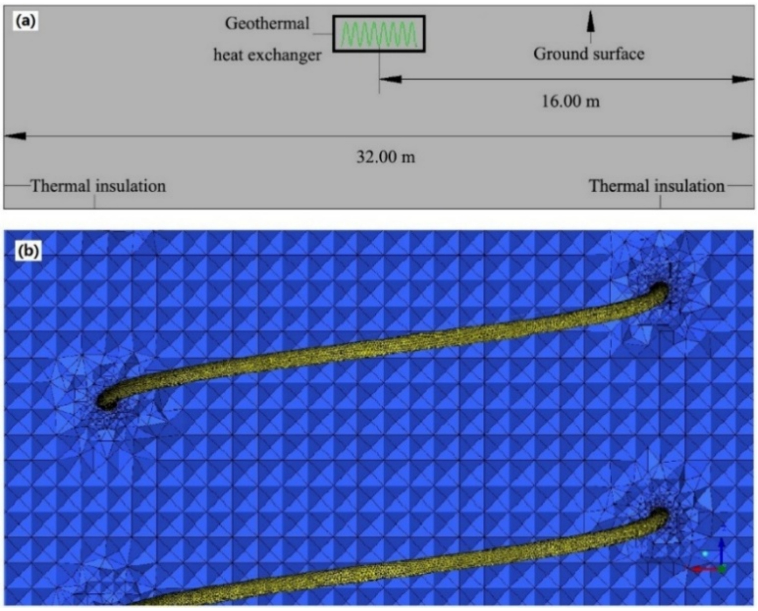

Figure 8 Illustration of the heat injection rate during the cooling operation

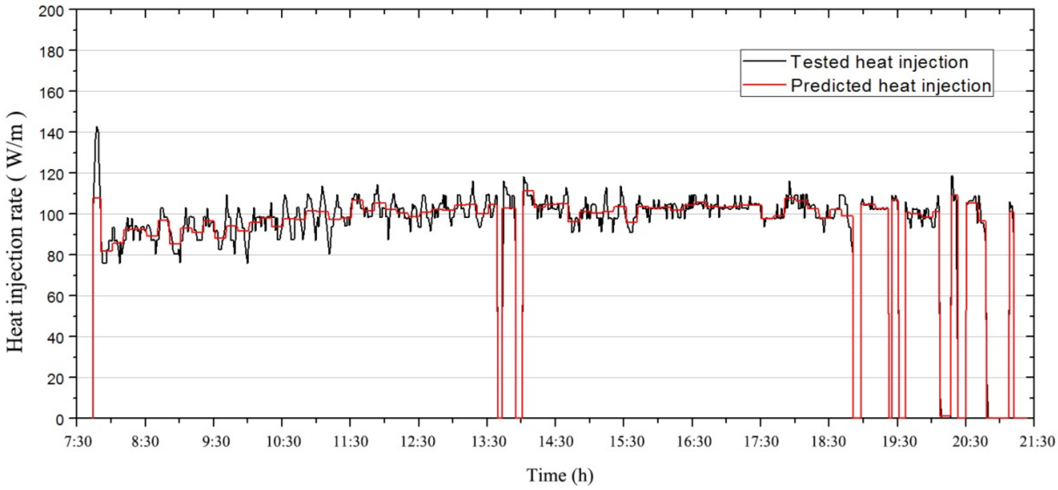

Figure 9 Soil temperature determined by experiment test and analytical calculation

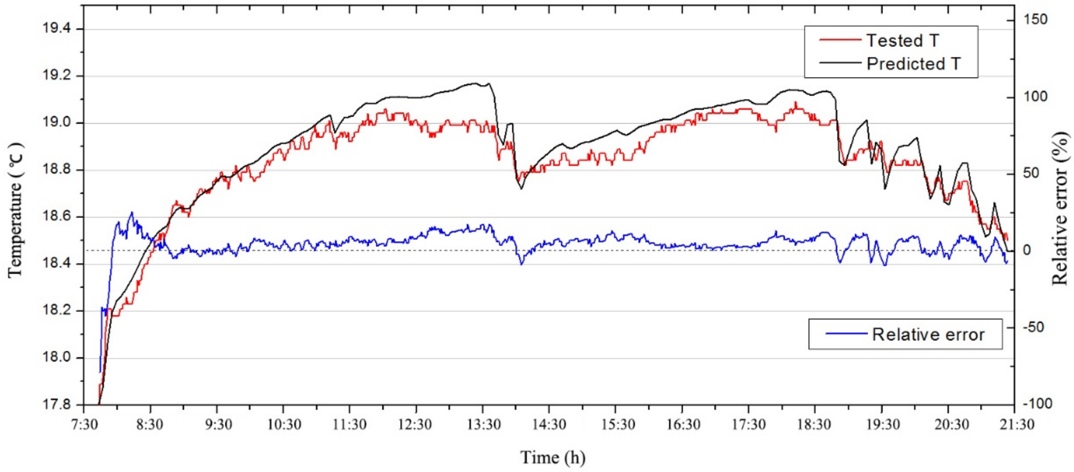

Figure 10 Variations of dimensionless temperature responses calculated by analytical and numerical methods with ***Fo*** with different numbers of coils

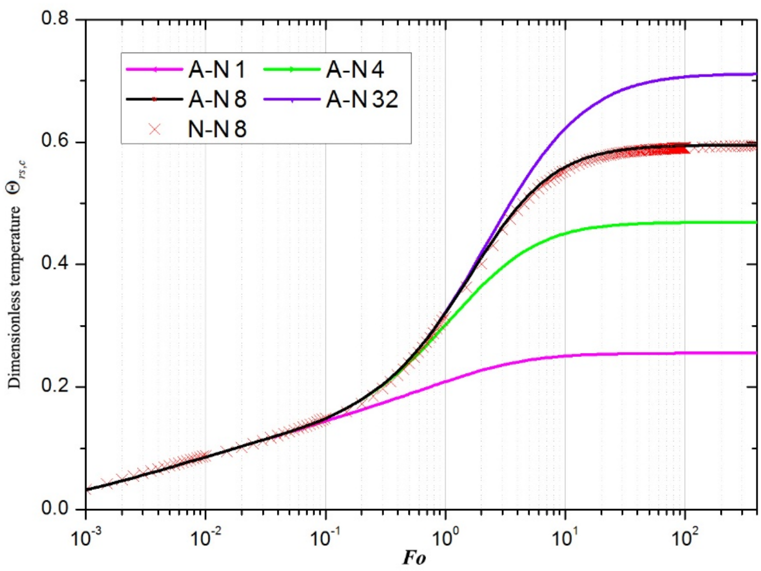

Figure 11 Temperature profiles along the axial direction with different ***Fo*** (with x=0 and z=0.6 m).

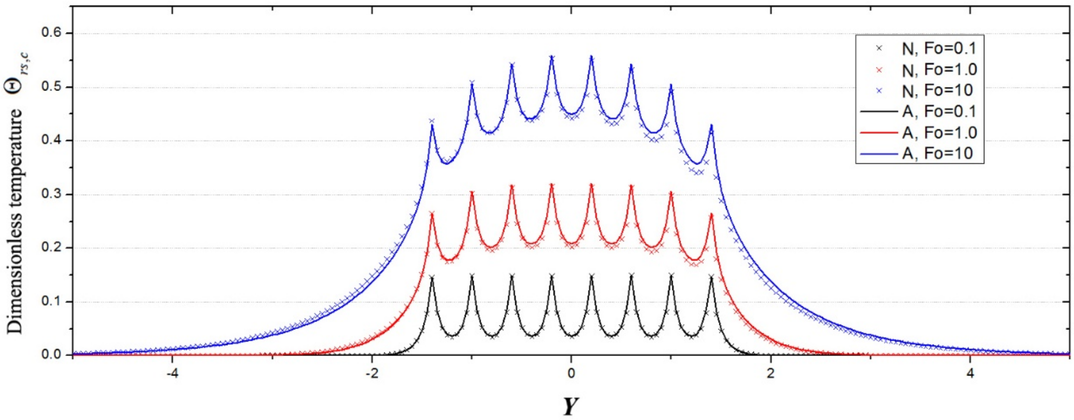

Figure 12 Temperature response calculated by analytical and numerical method with sinusoidal surface temperature (with x=0, y=1.2 and z=0.6m).

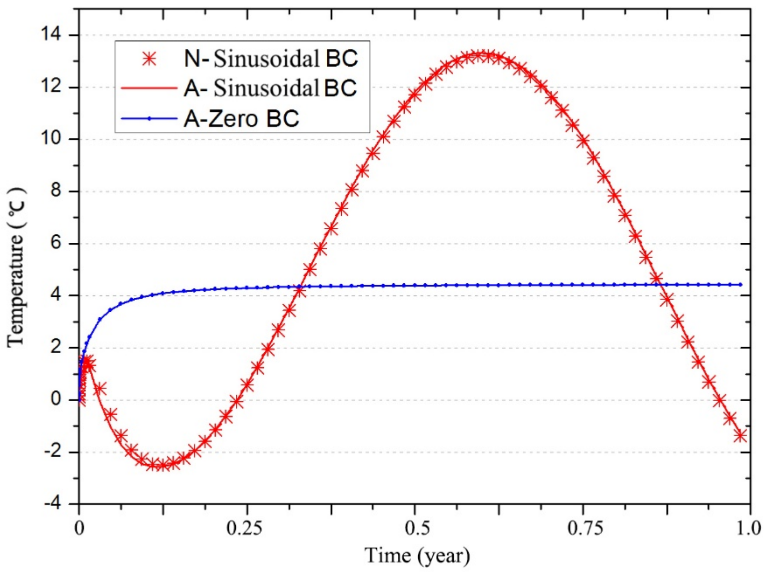

Figure 13 Annual climatic data, recorded by the climatic station, used as boundary conditions in the simulations

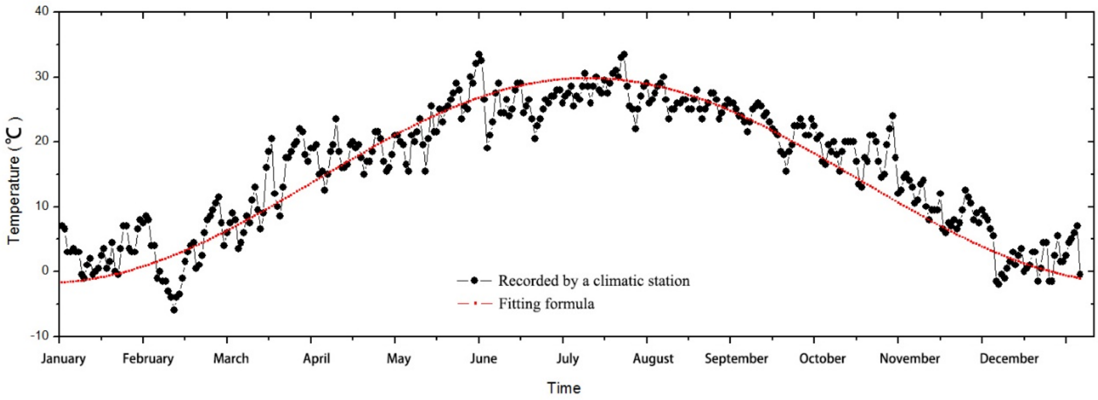

Figure 14 Illustration of the heat injection and extraction in one year

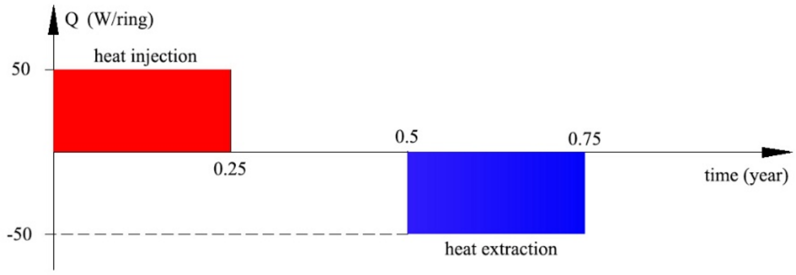

Figure 15 Arrangement of monitoring points and the vertical heat exchanger.

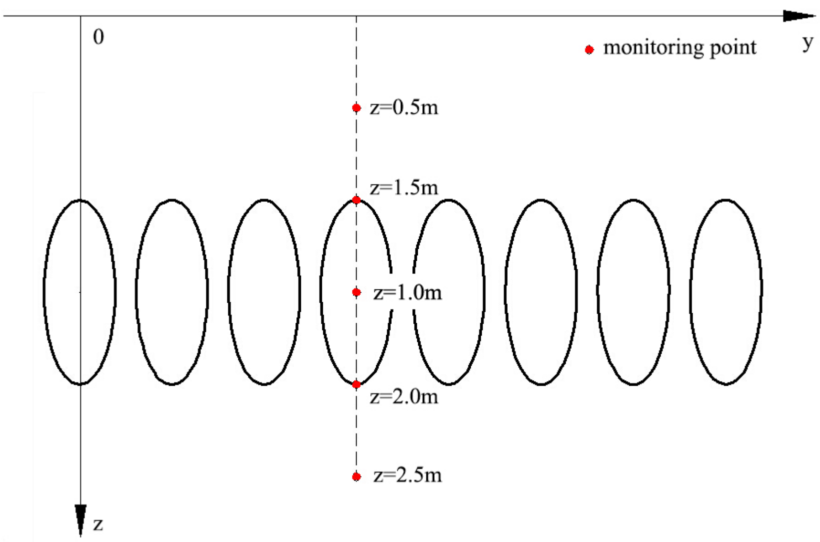

Figure 16 Soil temperature variation at different depths under sinusoidal surface temperature without heat source influence (with x=0m and y=1.2m)

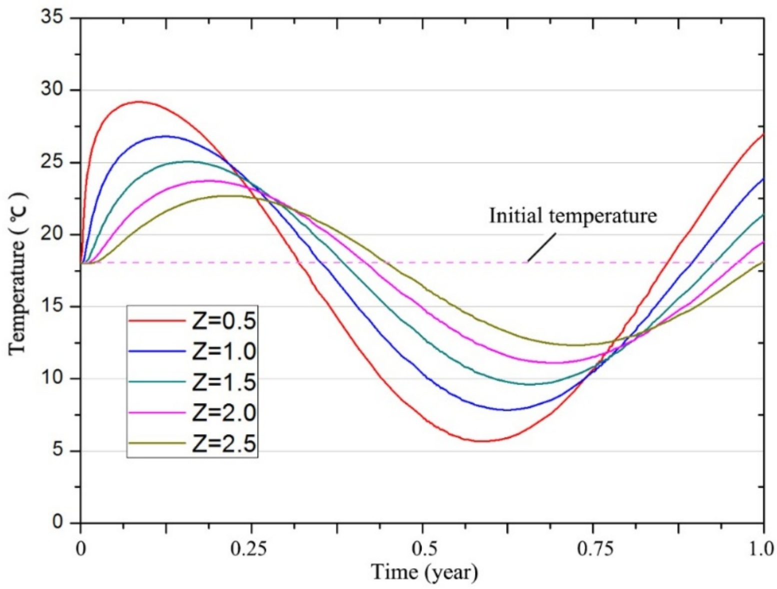

Figure 17 Soil temperature variation at different depths under constant surface temperature with heat injection/extraction (with x=0m and y=1.2m).

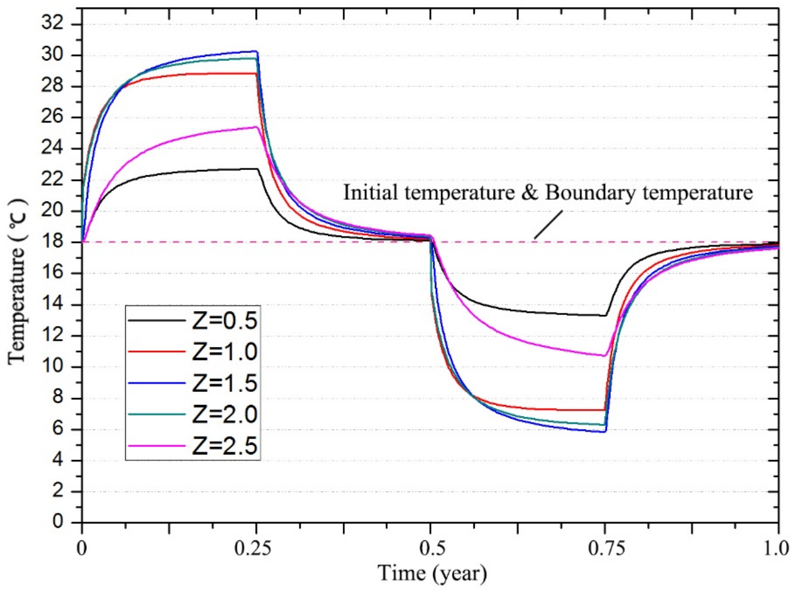

Figure 18 Soil temperature variation at different depths under sinusoidal surface temperature with heat injection/extraction (with x=0m and y=1.2m).

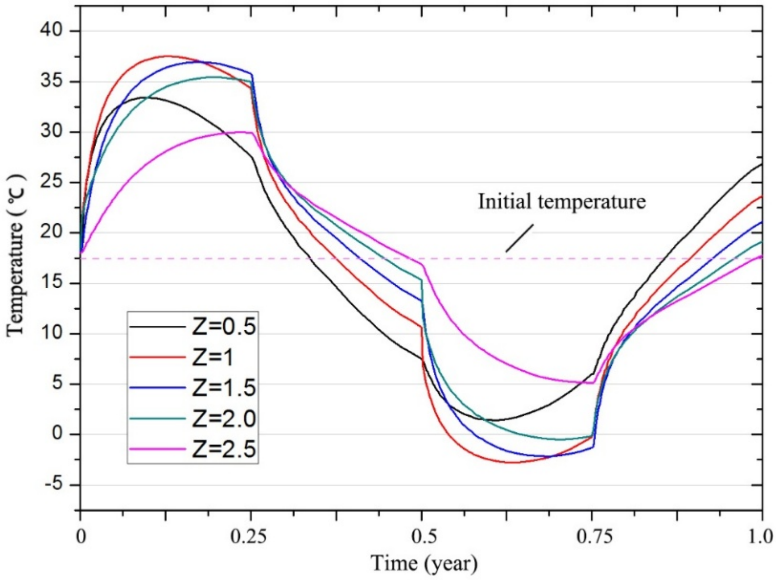

Reference

[1] H. Yang, P. Cui, Z. Fang, Vertical-borehole ground-coupled heat pumps: a review of models and systems, Applied Energy, 87(1) (2010) 16-27.

[2] P. Cui, J. Yang, Y. Lin, Z. Fang, Investigating the Thermal Performance of Horizontal Slinky Ground Heat Exchangers for Geothermal Heat Pump, in: Proceedings of the 8th International Symposium on Heating, Ventilation and Air Conditioning, Springer, 2014, pp. 73-83.

[3] C. Rousseau, J.-L.C. Fannou, L. Lamarche, M. Ouzzane, S. Kajl, Modeling and experimental validation of a transient direct expansion geothermal heat exchanger, Geothermics, 57 (2015) 95-103.

[4] J.-L. Fannou, C. Rousseau, L. Lamarche, K. Stanislaw, Experimental analysis of a direct expansion geothermal heat pump in heating mode, Energy and Buildings, 75 (2014) 290-300.

[5] D. Wang, L. Lu, W. Zhang, P. Cui, Numerical and analytical analysis of groundwater influence on the pile geothermal heat exchanger with cast-in spiral coils, Applied Energy, (2015).

[6] M. Li, A.C.K. Lai, New temperature response functions (G functions) for pile and borehole ground heat exchangers based on composite-medium line-source theory, Energy, 38(1) (2012) 255-263.

[7] Y. Man, H.X. Yang, N.R. Diao, P. Cui, L. Lu, Z.H. Fang, Development of spiral heat source model for novel pile ground heat exchangers, Hvac&R Research, 17(6) (2011) 1075-1088.

[8] H. Demir, A. Koyun, G. Temir, Heat transfer of horizontal parallel pipe ground heat exchanger and experimental verification, Applied Thermal Engineering, 29(2) (2009) 224-233.

[9] P.M. Congedo, G. Colangelo, G. Starace, CFD simulations of horizontal ground heat exchangers: A comparison among different configurations, Applied Thermal Engineering, 33-34 (2012) 24-32.

[10] P. Cui, D. Wang, J. Yang, N. Diao, Numerical simulation and experimental verification of horizontal ground heat exchangers, in: 12th International Conference on Sustainable Energy technologies Hong Kong, 2013.

[11] L. Ingersoll, H. Plass, Theory of the ground pipe heat source for the heat pump, ASHVE transactions, 47(7) (1948) 339-348.

[12] V. Mei, Heat pump ground coil analysis with thermal interference, Journal of solar energy engineering, 110(2) (1988) 67-73.

[13] H. Li, K. Nagano, Y. Lai, A new model and solutions for a spiral heat exchanger and its experimental validation, International Journal of Heat and Mass Transfer, 55(15-16) (2012) 4404-4414.

[14] Z. Xiong, D.E. Fisher, J.D. Spitler, Development and validation of a Slinky™ ground heat exchanger model, Applied Energy, 141 (2015) 57-69.

[15] S.J. Self, B.V. Reddy, M.A. Rosen, Geothermal heat pump systems: status review and comparison with other heating options, Applied Energy, 101 (2013) 341-348.

[16] Z. Xiong, E.S. Lee, Development of a Horizontal Slinky Ground Heat Exchanger Model, ASHRAE Transactions, 119 (2013) 1G.

[17] P. Cui, X. Li, Y. Man, Z. Fang, Heat transfer analysis of pile geothermal heat exchangers with spiral coils, Applied Energy, 88(11) (2011) 4113-4119.

[18] K.D. Cole, J.V. Beck, A. Haji-Sheikh, B. Litkouhi, Heat Conduction Using Green’s Functions, Taylor & Francis, 2010.

[19] S. Sanaye, B. Niroomand, Horizontal ground coupled heat pump: Thermal-economic modeling and optimization, Energy conversion and management, 51(12) (2010) 2600-2612.

[20] H.S. CARSLAW, Conduction of heat in solids.